American Mineralogist, Volume 103, pages 197–206, 2018

Laboratory and field characterization of visible to near-infrared spectral reflectance of nitrate minerals from the Atacama Desert, Chile, and implications for Mars

Fan Wang[1,2], Brenda B. Bowen[3,*,†], Ji-Hye Seo[4], and Greg Michalski[2,4]

[1]School of Environment and Energy, Peking University Shenzhen Graduate School, Shenzhen, Guangdong 518055, China
[2]Department of Earth, Atmospheric and Planetary Sciences, Purdue University, West Lafayette, Indiana 47907, U.S.A.
[3]Department of Geology and Geophysics, University of Utah, Salt Lake City, Utah 84112, U.S.A.
[4]Department of Chemistry, Purdue University, West Lafayette, Indiana 47907, U.S.A.

Abstract

Large amounts of nitrate salts occur in very specific environments and somewhat rare hyper-arid conditions, which may provide clues to fundamentally different nitrogen cycling and life survival mechanisms. Remote detection of ancient and modern nitrates on Earth and on other planetary bodies where they may occur requires a detailed understanding of their visible to near infrared (VNIR) spectral signatures. This study explores the VNIR spectral characteristics of several synthetic nitrate salts, sulfate minerals, and nitrate-bearing field samples from the Atacama Desert, Chile, to identify diagnostic spectral features of nitrate and possible interferences from other coexisting minerals. Results indicated that most of the nitrate salts have characteristic absorptions around 1.81, 1.94, 2.06, 2.21, and 2.42 μm. A significant positive correlation exists between the continuum-removed band depths of the 2.42 μm absorption and nitrate contents for the Atacama regolith samples, especially for samples with >10 wt% nitrate. The five absorption features of nitrate in the field spectra collected from multiple nitrate-rich regions in the Atacama Desert were then evaluated to determine the variabilities in these features in natural settings, while the band depths of 2.42 μm absorption were further calculated on the continuum-removed field spectra to estimate the nitrate abundances at the study sites. This work will supplement spectral libraries where nitrate spectra are lacking and have implications for future comparisons to planetary spectra to search for potentially life-related nitrate on Mars.

Keywords: Nitrate, Atacama Desert, Mars, visible to near infrared reflectance; Earth Analogs for Martian Geological Materials and Processes

Introduction

The Atacama Desert in northern Chile has been proposed as an important Mars analog due to its hyper-arid climate (Navarro-González et al. 2003). The hyper-aridity in the core of the Atacama Desert is the combined result of the rain shadow effects created by the Coastal Range and the Andes, the cold upwelling Peru Current, and the south Pacific subtropical anticyclone (Houston and Hartley 2003; Houston 2006). The Atacama is known to have highly saline soils containing the largest nitrate deposits in the world (Ericksen 1981), which is unique and mainly due to that the hyper-arid climate minimizes leaching losses and preserves nitrate and other soluble salts, such as chloride, sulfate, and perchlorate. While the hyper-aridity stabilizes the saline soils in the Atacama, the origins of massive soluble salts were long disputed before recent isotopic studies definitely attributed these soluble salts to atmospheric origins (Bao and Gu 2004; Bao et al. 2004; Michalski et al. 2004; Wang et al. 2016). Oxides of nitrogen, sulfur, and chlorine in the atmosphere can be oxidized via photochemical pathways (i.e., chemical reactions caused by light) into their stable end products as nitrate, sulfate, and perchlorate, respectively, which can subsequently be deposited onto the ground surface (Seinfeld and Pandis 2006). As recent development of triple oxygen isotope analysis allowed the source apportionment of soluble salts in the soil based on distinctive oxygen isotope signatures in different sources, the Atacama salts were revealed to have similar oxygen isotope compositions to their atmospheric equivalents, suggesting their predominant origin from atmospheric deposition. Indeed, in hyper-arid environments such as the Atacama, where biological and hydrological activities should be extremely low, atmospheric deposition, especially dry deposition, may be one of the main processes that control surface geomorphology (Ewing et al. 2006). The successive detection of sulfate, chloride, and perchlorate on the surface of Mars (Squyres et al. 2004; Osterloo et al. 2008; Hecht et al. 2009), similar to the existence of chloride, perchlorate, and sulfate deposits in the Atacama, hints that analogous deposition processes may be occurring on Mars.

Whether there are also nitrate deposits occurring on Mars as in the Atacama is of great interests to the scientific community because nitrate is an important part of biogeochemical cycling on Earth and may be indicative of past life on Mars. Several studies have proposed mechanisms that could lead to photochemical production of nitrate in a martian atmosphere (Yung et al. 1977; Nair et al. 1994) and possible incorporation of nitrate into the martian regolith (Banin et al. 1997; Mancinelli 1996). Nevertheless, the

* E-mail: brenda.bowen@utah.edu
† Special collection papers can be found online at http://www.minsocam.org/MSA/AmMin/special-collections.html.

0003-004X/18/0002–197$05.00/DOI: https://doi.org/10.2138/am-2018-6141

search of nitrate on Mars had proved to be very difficult until the Sample Analysis at Mars (SAM) instrument suite on the Mars Science Laboratory (MSL) Curiosity rover recently detected NO that was believed to be released from the breakdown of nitrates during pyrolysis (Stern et al. 2015). However, other nitrogen-containing compounds could also release NO as samples were heated by SAM, which complicates interpretations of nitrate abundances in martian soils from SAM analysis. In addition, SAM analysis is confined to a relatively small region that is limited by the activities of the Curiosity rover and the time and costs of each analysis. Instead, orbital spectral sensors can provide an important tool for investigating planetary-scale presence or absence of nitrate on Mars. However, use of these sensors requires a detailed understanding of the spectral characterization of nitrate minerals and how they vary in natural heterogeneous environments.

Spectral characterization of nitrate has been previously reported (Hovis 1966; Ericksen and Mrose 1970; Harris et al. 1990; Sutter et al. 2007), and there have been several trials using nitrate spectral characteristics to determine nitrate in soil or vegetation leaves (Ehsani et al. 2001; Boonmung and Riley 2003; Jahn et al. 2006). However, these trials were primarily laboratory investigations focusing on representative spectral features in the mid-infrared region, providing limited comparisons for martian sensors that usually measure reflectance in the visible to near infrared (VNIR) region. To our knowledge, only two works to date (Sutter et al. 2007; Cloutis et al. 2016) discussed the possibility of nitrate detection using VNIR hyperspectral remote sensing techniques on Mars. Sutter et al. (2007) systematically compared the laboratory spectra (0.35–25 μm) of several minerals commonly existing in the Atacama Desert, including nitratine ($NaNO_3$), to the remotely sensed spectra of the martian soil to help identify mineral compositions, but they were mainly concentrated on infrared analysis of Atacama soils with very little attention to nitrate, especially less attention extended to nitrate detection on Mars. Cloutis et al. (2016) measured the reflectance spectra (0.35–20 μm) of synthetic KNO_3, $NaNO_3$, and NH_4NO_3 compounds and summarized the current and future hyperspectral imaging systems that could be adopted for the search of nitrate on Mars, but they rarely addressed how nitrate spectra are impacted by interferences from coexisting minerals. In summary, still missing are VNIR spectra of a wide selection of nitrate compounds in spectral libraries, understanding of how the nitrate absorptions are interfered by coexisting minerals, and field assessments to couple laboratory investigations with remote sensing data (Moorcroft et al. 2001; Sinfield et al. 2010). Therefore, this study is designed to characterize the VNIR absorption features of nitrate, evaluate the interferences of nitrate absorptions from coexisting minerals, and develop a scheme to detect the presence of nitrate and quantify the nitrate abundances based on reflectance spectra at the field scale, which will provide perspectives into the nitrate search via remote sensing on Mars and in other similar environments.

Methods

Laboratory spectra collection

Several pure synthetic nitrate salts and sulfate minerals (potentially interfering minerals for nitrate spectral characterization) were obtained for laboratory spectral analysis. Sixteen reagent-grade metal nitrate salts (Table 1) and mirabilite ($Na_2SO_4 \cdot 10H_2O$) were purchased from authorized commercial retailers. Though some of the 16 metal nitrates might be rare in most terrestrial systems, they were included to supplement the database and investigate whether characteristic nitrate features or spectral shifts are prominent for a wide selection of nitrate compounds. Delicate platy darapskite crystals ($Na_3NO_3SO_4 \cdot H_2O$) were precipitated out through gradual evaporation of the mixture of saturated $NaNO_3$ and Na_2SO_4 solutions under warm ambient temperature (approximately 20 °C). Darapskite and mirabilite samples were heated in a muffle furnace at 60 °C for 2 h to remove any adsorbed water before measurements to look at the characteristic absorption features in anhydrous forms of minerals. These salt or mineral samples were all gently ground to powders of homogenous grain sizes (<0.18 mm) for further analysis.

Atacama regolith samples were collected from two trenches in the Baquedano region, called "long trench" (LT) and "small trench" (ST), respectively, and one incised lahar paleosediment profile in the Chug-Chug geoglyphs field, called "Chug-Chug paleosediment" (CCP). The LT site (22.88°S, 69.64°W, 1500 m a.s.l.) is a 225 cm deep trench stretching several kilometers [see more details in Wang et al. (2015)], while the ST site (22.83°S, 69.72°W, 1501 m) is a ~2 m long and 2.35 m deep trench unit. These two trench sites are located in the Baquedano basin that is characterized by flat, rugged, and barren alluvial surfaces, receiving <0.4 mm precipitation annually (Houston 2006). No erosional evidence was observed at either trench site, and all the regolith material were loosely cemented such that they could be sampled with hand shovels. The CCP site (22.04°S, 69.13°W, 2423 m) is a 4 m high profile located in an ancient riverbed with sediment channels preserved in the upper stratum and a spring nearby with sparse vegetation. All horizons of the CCP profile consisted of well-cemented rock-like sediment, requiring electric saws for sampling. The trenches and paleosediment outcrop were sampled from the bottom (2–4 m) to the surface at ~5 cm vertical resolution, totaling 43, 55, and 72 samples from the LT, ST, and CCP profiles, respectively.

The powdery salts and minerals, and intact regolith samples were analyzed in the laboratory at Purdue University using an ASD FieldSpec 3 reflectance spectrometer (Analytical Spectral Devices Inc., Boulder, Colorado) that measures reflectance from 0.35–2.5 μm. Reflectance was measured relative to a white reflectance standard Spectralon plate (Labsphere Inc., North Sutton, U.K.) using the instrument's fiber optic contact probe that has a 1 cm diameter spot size and 8° field of view. Lab measurements were made in a dark room using artificial illumination of white light emitted from a tungsten filament lamp (~3400 K color temperature). The wavelength scanning interval is 1.4 nm in the spectral range of 0.35–1.0 μm and 2 nm in the spectral range of 1.0–2.5 μm, while the spectral resolution ranges from 3–10 nm. Thirty scan acquisitions were set to yield an average spectrum for each spectral measurement during the indoor operation to improve the signal-to-noise ratio. Continuum was further removed of the measured

Table 1. Positions of the 1.5–2.5 μm absorption band minima for metal nitrate salts (uncertainties ≤10 nm)

Nitrate salts	Minima of absorption bands (μm)
	Anhydrous nitrate
KNO_3	1.83, 1.95 (shoulder), 1.97, 2.06 (shoulder), 2.10, 2.20 (shoulder), 2.25, 2.42 (shoulder), 2.47
$NaNO_3$	1.80, 1.92 (shoulder), 1.94, 2.04 (shoulder), 2.06, 2.18 (shoulder), 2.22, 2.43, 2.47 (shoulder)
$Pb(NO_3)_2$	1.83, 1.98, 2.10, 2.26, 2.43 (shoulder), 2.47
$Th(NO_3)_4$	1.80 (shoulder), 1.86, 1.95, 2.01, 2.06, 2.12, 2.17, 2.25 (shoulder), 2.29, 2.33 (shoulder), 2.45
$LiNO_3$	1.75, 1.81, 1.98, 2.04 (shoulder), 2.17, 2.45
	Hydrated nitrate
$Cu(NO_3)_2 \cdot H_2O$	1.69 (shoulder), 1.80, 1.95, 2.00, 2.18 (shoulder), 2.38 (shoulder), 2.50
$Cd(NO_3)_2 \cdot 4H_2O$	1.74, 1.80, 1.94, 1.98 (shoulder), 2.08, 2.17 (shoulder), 2.42, 2.50
$Zr(NO_3)_4 \cdot 5H_2O$	1.79 (shoulder), 1.92, 2.28 (shoulder), 2.50
$Co(NO_3)_2 \cdot 6H_2O$	1.72, 1.80, 1.95, 2.22, 2.38
$La(NO_3)_3 \cdot 6H_2O$	1.78, 1.94, 2.19, 2.47 (broad)
$Mg(NO_3)_2 \cdot 6H_2O$	1.55 (shoulder), 1.74 (shoulder), 1.78, 1.95, 2.15 (shoulder), 2.24 (shoulder), 2.40 (shoulder), 2.50
$Ni(NO_3)_2 \cdot 6H_2O$	1.62 (shoulder), 1.83, 1.95, 2.06 (shoulder), 2.41, 2.50
$UO_2(NO_3)_2 \cdot 6H_2O$	1.74, 1.93 (shoulder), 1.99, 2.19 (shoulder), 2.42 (shoulder), 2.50
$Fe(NO_3)_3 \cdot 7H_2O$	1.79 (shoulder), 1.94, 2.50
$Al(NO_3)_3 \cdot 9H_2O$	1.76 (shoulder), 1.94, 2.05 (shoulder), 2.37 (shoulder), 2.498
$Zn(NO_3)_2 \cdot 10H_2O$	1.72 (shoulder), 1.82 (shoulder), 1.95, 2.21 (shoulder), 2.36 (shoulder), 2.50

reflectance spectra by dividing the reflectance values of an established convex hull into the actual reflectance spectrum (Kokaly and Clark 1999) to isolate the absorption features. The absorption band depth was calculated by subtracting the relative reflectance value at the band minimum of each absorption feature from 1 in the continuum-removed spectrum.

In addition, one gram of each regolith sample was homogenized, ground by ball mill or hand, and vortexed to extract soluble salts with 45 mL Milli-Q Millipore-water (ultrapure >16MΩ). The anion (chloride, nitrate, and sulfate) contents in the extracts were analyzed using a Dionex-500 ion chromatography with suppressed conductivity detection (Dionex Corp., Sunnyvale, California). Blank controls and external standard calibration were performed for quality control and assurance. The measurement uncertainties for anion contents were typically <5% based on replicate analysis of standards and calibrations. Correlation analysis between the absorption band depths and anion contents of samples from the three profiles (LT, ST, and CCP) was performed using the statistical software package PASW Statistics 18.0 (SPSS Inc., Chicago, Illinois).

Field spectra collection

In situ field-based spectra were collected by the ASD FieldSpec 3 reflectance spectrometer using a pistol grip with the attached fiber optic cable for one soil pit (Baquedano pit 1), three mine tailings (Baquedano mine, Sierra Gorda mine and Tama mine), and two salars (Salar de Carmen and Salar de Grande). These sites were selected to collect field spectra due to that their textural and environmental characteristics suggested possible presence of surface nitrate efflorescent salts. The measurements were taken at a distance of 5–10 cm from the samples around noon on clear days, and the white reflectance standard Spectralon plate was measured every 2–3 min to minimize the effects of changing illumination and meteorological conditions. One hundred scan acquisitions were set to yield an average spectrum for each field spectral measurement to improve the signal-to-noise ratio. In addition, 6 returned field samples from Baquedano pit 1, 4 from Baquedano mine, 8 from Sierra Gorda mine, and 14 from Tama mine were measured for reflectance in the laboratory and their laboratory spectra were compared to the field spectra to check their consistence.

The Baquedano pit 1 site (22.98°S, 69.84°W, 1400 m a.s.l), close to the LT and ST sites (~20 km distance), is a ~2 m deep pit located in an alluvial fan that lacks surface erosion features but has a ~15 cm deep gypsum layer developed below the surface in the Baquedano region (Fig. 1a). The weathered surface of the pit face was removed to expose a fresh surface before 23 field spectra were collected.

The Baquedano mine site (23.11°S, 69.91 °W, 1432 m) is near a deserted nitrate mine, and its surface of a reddish appearance is highly disturbed with big rocks exposed (Fig. 1b). The Sierra Gorda nitrate mine site (23.07°S, 69.49°W, 1420 m) is located in the Sierra Gorda region with a mine tailing ~10 m high and ~3000 m ×1200 m in size (Fig. 1c). The Tama mine site (20.52°S, 69.77°S, 999 m) is in a hilly terrain with weathered broken rocks in the surroundings and a gentle hill slope (Fig. 1d) and visually similar to the Burns Cliff within Endurance Crater on Mars (Watters et al. 2011). Field spectral measurements of 21, 26, and 27 were conducted on the tops and along the cross sections of the Baquedano, Sierra Gorda and Tama mine tailing profiles, respectively.

The Carmen site (23.65°S, 70.27°W, 524 m) is located on the western side of the Salar de Carmen, a closed basin at the terminus of the broad, transverse, debris-filled Baquedano valley drainage (Ericksen 1981); nitrate minerals are known to periodically accumulate on the salar's surface (Whitehead 1920). 53 field spectra were collected in total along two ~100 m long representative transects that are covered with soft, flat, and yellowish surface (Fig. 1e). The Grande site (21.22°S, 69.90°W, 800 m) is located on the southeastern rim of the Salar de Grande, a terminal basin filled with massive salt minerals, mainly halite (NaCl). 74 field spectra of the surfaces were taken along a ~100 m long transect over which the barren ground covered with 0.5–1 cm reddish to tannish pebbles abruptly transitions to a hummocky ground with a relief of 50 cm. The hummocky ground is mostly covered with biological crusts, while barren depression pits (~2–5 m in diameter) filled with white salt nodules (mainly halite) were sparsely scattered across the hummocky ground (Fig. 1f).

Results and Discussion

Nitrate characterization

The 16 pure nitrate salts are divided into two groups based on their hydration states and their 0.35–2.5 μm reflectance spectra are shown in Figure 2, while the positions of the absorption band

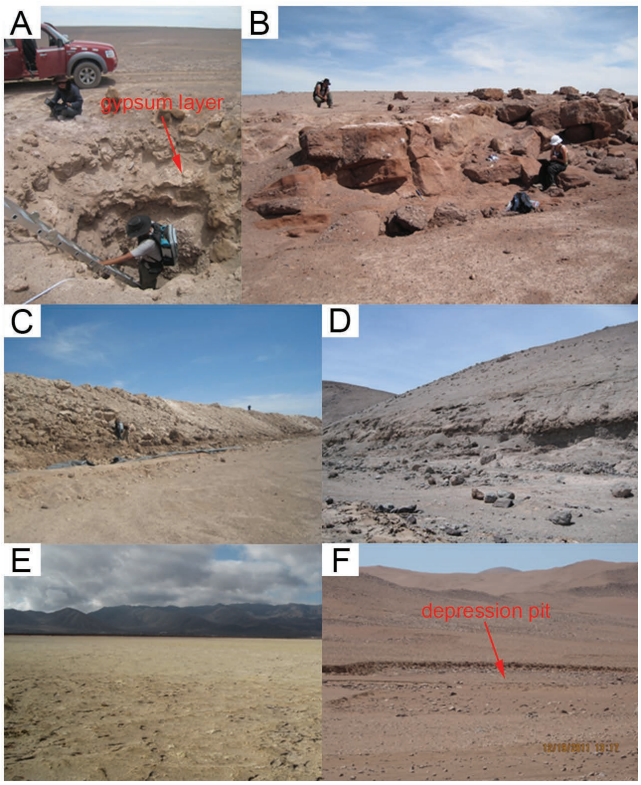

Figure 1. Field pictures of Baquedano pit 1 (**a**), Baquedano mine (**b**), Sierra Gorda mine (**c**), Tama mine (**d**), Salar de Carmen (**e**), and Salar de Grande (**f**) sites where the field reflectance spectra were collected.

minima in the 1.5–2.5 μm region are listed in Table 1. Sutter et al. (2007) reported that various N-O overtones/combinations could cause VNIR absorptions around 1.81, 1.94, 2.06, 2.21, and 2.42 μm (Table 2), while Cloutis et al. (2016) revealed that the positions of the absorption band minima might vary slightly in different minerals. The spectra of anhydrous $NaNO_3$ and KNO_3 salts in this study are similar to the spectrum of niter (KNO_3) archived in the USGS spectral library by Clark et al. (2007) (Fig. 2a and Table 1) and the observations for $NaNO_3$ and KNO_3 by Sutter et al. (2007) and Cloutis et al. (2016). They all show prominent absorptions around 1.81, 1.94, 2.06, 2.21, and 2.42 μm despite the changes in the positions of band minima and some being in the form of shoulders. These five characteristic absorption features are relatively weak but present in the spectra of $Pb(NO_3)_2$ and $Th(NO_3)_4$, and the long-wavelength absorption features are more easily identified (Fig. 2a and Table 1). $LiNO_3$ has sharp and broad absorptions around 1.4 and 1.9 μm (Fig. 2a) that are diagnostic of water molecules (Table 2; Hunt 1977), likely due to the hygroscopic capacity of $LiNO_3$ that leads to the presence of adsorbed water. The 1.81, 2.21, and 2.42 μm features are also discernible in the spectrum of $LiNO_3$, while the 1.94 and 2.06 μm features are merged into the broad ~1.9 μm water absorption band, showing only small shoulders. In Figure 2b, the hydrated salts all have significant water absorption bands around 1.4 and 1.9 μm, but the depth and width of water bands were not observed to relate to the changes in hydration states. $Cu(NO_3)_2 \cdot H_2O$, $Fe(NO_3)_3 \cdot 7H_2O$, and $Zn(NO_3)_2 \cdot 10H_2O$ have strong absorptions over the 0.35–2.5 μm spectral range likely owing to crystal

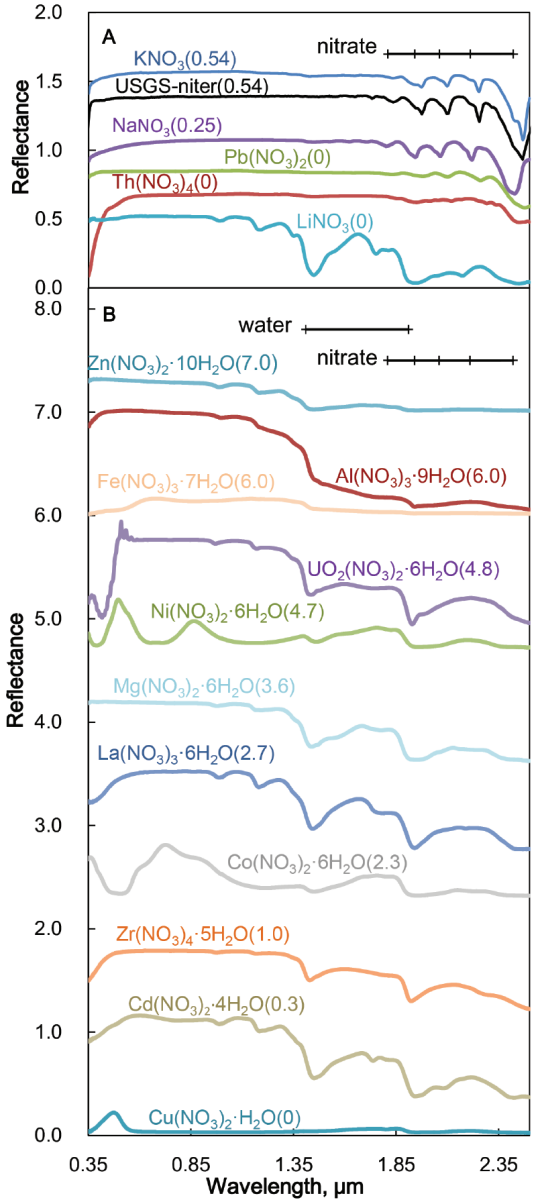

Figure 2. Laboratory reflectance spectra of metal nitrate salts without water of hydration (**a**; except $LiNO_3$, see text) and with water of hydration (**b**). The USGS-niter spectrum is for the mineral niter (KNO_3) from the USGS spectral library archived by Clark et al. (2007). The positions of nitrate and molecular water absorptions are indicated by the bars on the top of the charts. For clarity, the spectra are offset by an additive factor listed in the parentheses after the mineral names or chemical formulas in the charts.

field effects of their metal ions (Hathaway et al. 1963; Hunt 1977), while the strong absorptions by $Al(NO_3)_3·9H_2O$ in the 1.0–2.5 µm range are likely attributed to the overtones and combinations of water molecules as well as the Al-OH vibrations. For other hydrated salts in Figure 2b, most of the 1.94, 2.06, and 2.21 µm absorption features of nitrate are strongly influenced by the 1.9 µm water absorption to only show shoulders, while small absorptions or inflections are typically noticeable around 1.81 and 2.42 µm despite some shifts in the absorption feature

Table 2. Modes and positions of 0.35–2.5 µm absorption features relevant to this study (summarized from previous studies)

Mode	Position (µm)
Water molecule (Hunt 1977)	
$2v_1+v_3$	0.942
$v_1+v_2+v_3$	1.135
v_1+v_3	1.38
$2v_1+v_3$	1.454
v_2+v_3	1.875
Hydroxyl (Hunt 1977; Clark et al. 1990)	
$3v_{OH}$	0.95
$2v_{OH}$	1.4
Al-OH	2.2
Mg-OH	2.3
Fe-OH	2.29
Nitrate (Sutter et al. 2007; Cloutis et al. 2016)	
$4v_3$	1.81
$3v_3+v_2+v_L$	1.94
$3v_3+v_4$	2.06
$2v_3+2v_2$	2.21
$3v_3$	2.42
Sulfate (Gendrin et al. 2005)	
Association of S-O bonds and H_2O	2.4
Carbonate (Clark et al. 1990)	
v_1+3v_3	1.88
$2v_1+2v_3$	2.00
$v_1+2v_3+v_4$ or $3v_1+2v_4$	2.17
$3v_3$	2.31

center positions. The differences in the size or center position of absorption features of different nitrate salts (Fig. 2) are likely due to distinct ion pairing effects of different metal ions (Xu et al. 2008). Therefore, the five absorption features at 1.81, 1.94, 2.06, 2.21, and 2.42 µm are diagnostic nitrate features, but may overlap with water bands and may also be displaced depending on the cations in the nitrate salts.

There are some unique minerals that coexist with nitrate minerals in the Atacama (Ericksen 1981) and are likely to coexist in other similar hyper-arid environments, which may interfere with the nitrate absorptions at some wavelengths. Sulfate minerals such as gypsum ($CaSO_4·2H_2O$) and anhydrite ($CaSO_4$) are ubiquitously found in the Atacama, which can be one of the major mineral groups coexisting with nitrate in hyper-arid environments (Ericksen 1981). The comparison of the spectra of the anhydrous and hydrated forms of two common Atacama sulfate minerals, mirabilite ($Na_2SO_4·10H_2O$) and darapskite ($Na_3NO_3SO_4·H_2O$), indicates that the hydrated forms have stronger absorption features than their anhydrous forms (Fig. 3). The reflectance spectrum of anhydrous Na_2SO_4 is nearly flat without absorptions in the VNIR region, suggesting that there are no characteristic absorptions by sulfate group in the VNIR region. No sulfate absorption feature in the VNIR region was also observed in the spectrum of anhydrite ($CaSO_4$) that was archived in the USGS spectral library (Clark et al. 2007). Crowley (1991) measured the VNIR spectrum of thenardite (Na_2SO_4) to find only two broad water bands near 1.4 and 1.9 µm, which, however, were likely accounted for by the presence of fluid inclusions and/or adsorbed water rather than the sulfate group. In addition, the reflectance spectrum of anhydrous darapskite ($Na_3NO_3SO_4$) is nearly identical to that of $NaNO_3$ (Fig. 3), also providing a line of evidence of the lack of absorption features for sulfate in the VINR region. The absence of sulfate absorption features in the VNIR region is likely because there are no overtone or combination features of sulfate in the VNIR region owing to the low frequencies of the fundamentals of sulfate in the

middle infrared region (Cloutis et al. 2006). Therefore, the VNIR absorption features in hydrated sulfate minerals are mainly due to the presence of water molecules or possible hydroxyl (OH). The differences between our spectra of mirabilite and anhydrous Na_2SO_4 showed the absorption bands centered at 0.97, 1.21 (with a shoulder), 1.48 (broad, with a shoulder), 1.75, 1.9 (broad), and 2.5 µm (Fig. 3), which are accounted for by the overtones and combinations of fundamental vibration modes of the water molecule and the association of S-O bonds and H_2O (~2.4 µm) (Table 2). For sulfate minerals with OH in the crystal structure, the overtones of OH stretching and combinational vibrations of OH stretching and metal-OH bending can also cause absorptions in the VNIR region as indicated in Table 2. These water molecule or OH-related absorptions in hydrated sulfate minerals may overlap with some of the nitrate absorption bands.

Previous studies suggested the major minerals of Atacama regoliths other than nitrate and sulfate minerals are: quartz (SiO_2), anorthite ($CaAl_2Si_2O_8$), albite ($NaAlSi_3O_8$), microcline ($KAlSi_3O_8$), hornblende [$(Ca,Na)_2(Mg,Fe,Al)_5(Al,Si)_8O_{22}(OH)_2$], and chlorine salts (e.g., halite NaCl and sodium perchlorate $NaClO_4$) (Ewing et al. 2006; Wang et al. 2015). Carbonate may also sporadically occur in some parts of the Atacama in the form of calcite ($CaCO_3$). The anhydrous forms of these major interference minerals except carbonate were shown to have no diagnostic absorptions in the VNIR region (Clark et al. 2007; Sutter et al. 2007; Hanley et al. 2015), though some hydrated forms may have absorptions overlapping nitrate features. Carbonate has relatively weak absorptions near 1.88, 2.00, and 2.17 µm overlapping with some nitrate absorption bands, but its most intense absorption occurring near 2.31 µm would not overlap the nitrate absorptions (Clark et al. 1990).

In summary, the characteristic nitrate absorption features around 1.81, 1.94, 2.06, 2.21, and 2.42 µm could mainly be interfered by adsorbed water or hydrated minerals, and therefore, careful inspections should be coupled with the VNIR spectral analysis. However, our measured spectrum of hydrated darapskite shows all of these five absorption bands despite the existence of water of hydration, suggesting the nitrate absorption bands may superimpose on water/metal-OH absorption bands to allow for the identification of nitrate via characteristic absorption features. Though hydrated minerals have been confirmed to exist widely in the hyper-arid settings such as the Atacama or similar planetary environments such as Mars, the interferences of water/metal-OH should depend on the nitrate contents and hydration status of individual samples, and the nitrate absorption features may stand out when high nitrate contents but low hydration degrees are present.

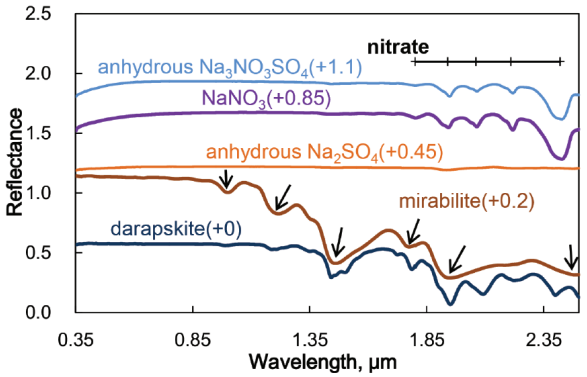

FIGURE 3. Comparison of laboratory reflectance spectra of the anhydrous and hydrated forms of two common Atacama sulfate minerals (i.e., mirabilite $Na_2SO_4 \cdot 10H_2O$ and darapskite $Na_3NO_3SO_4 \cdot H_2O$). The arrows delineate the water/hydroxyl-related absorption features. The positions of nitrate absorption features as shown in Table 2 are indicated by the bars on the top of the chart. For clarity, the spectra are offset by a factor (positive: additive) listed in the parentheses after the mineral names or chemical formulas in the chart.

Quantitative relationship between nitrate content and absorption band depth

The anion (chloride, nitrate, and sulfate) contents and laboratory spectra of all the regolith samples from the LT, ST, and CCP profiles are shown in Supplemental[1] Figures S1 and S2, respectively. The nitrate contents range from 0.4–8.3 wt% in the LT profile, 0–13.7 wt% in the ST profile, and 0.2–36.9 wt% in the CCP profile. Representative spectra are then selected based on spectral diversity and variety of nitrate content and presented in Figure 4. These spectra are relatively flat near 1.81 µm, but have absorption features around 1.9, 2.06 (shoulder), 2.21, and 2.42 µm. As the nitrate content increases, the 1.81, 2.06, and 2.42 µm absorptions become more conspicuous and significant, while the 1.9 and 2.21 µm absorptions had relatively small variations in band depths probably because these two absorptions are also accounted for by water/metal-OH (Fig. 4). For example, the sample with the second highest nitrate content (19.6 wt%) in the CCP profile starts to have distinct absorptions around 1.81 and 2.06 µm, and the 2.42 µm feature transitions from an inflection to a trough (Fig. 4c). Our observations are consistent with the demonstration by Hovis (1966) of prominent 1.81 and 2.42 µm absorption troughs for the sample with 15 wt% $NaNO_3$ compared to no significant absorptions at 1.81 µm and a downward line at 2.42 µm for the sample with 10–12 wt% $NaNO_3$. However, for the sample with the highest nitrate content (36.9 wt%), the center of the ~1.9 µm band occurs at ~1.94 µm, and the absorption band at ~2.21 µm becomes considerably sharper, probably due to the elevation in the contribution of nitrate relative to water/metal-OH to the absorptions (Fig. 4c). These changes are more pronounced in the continuum-removed spectra of the selected CCP samples for the characteristic nitrate absorption features (Figs. 5a–5d).

Correlation analysis indicated a significant positive correlation between nitrate contents and the 2.42 µm absorption band depths in the CCP profile ($n = 72$, Pearson correlation coefficient: 0.53, $p = 0.000$) (Table 3). However, the 2.42 µm absorption band depths remain relatively consistent when nitrate contents range from 0–10 wt% (Fig. 5f), and significant positive correlations are not observed in the LT and ST profiles that have much lower nitrate contents, suggesting that the 2.42 µm absorption feature is essentially sensitive to high nitrate contents. In addition, the wavelength position of the 2.42 µm band minima oscillated between 2.34 and 2.45 µm (Fig. 5e). Since the ~2.35 µm absorption could be attributed to metal-OH, the samples with the 2.42 µm band minima occurring at ~2.35 µm were excluded for further correlation analysis. Therefore, only the samples with nitrate contents >10 wt% and the band minima occurring at ~2.42 µm were adopted to further investigate the correlation between nitrate

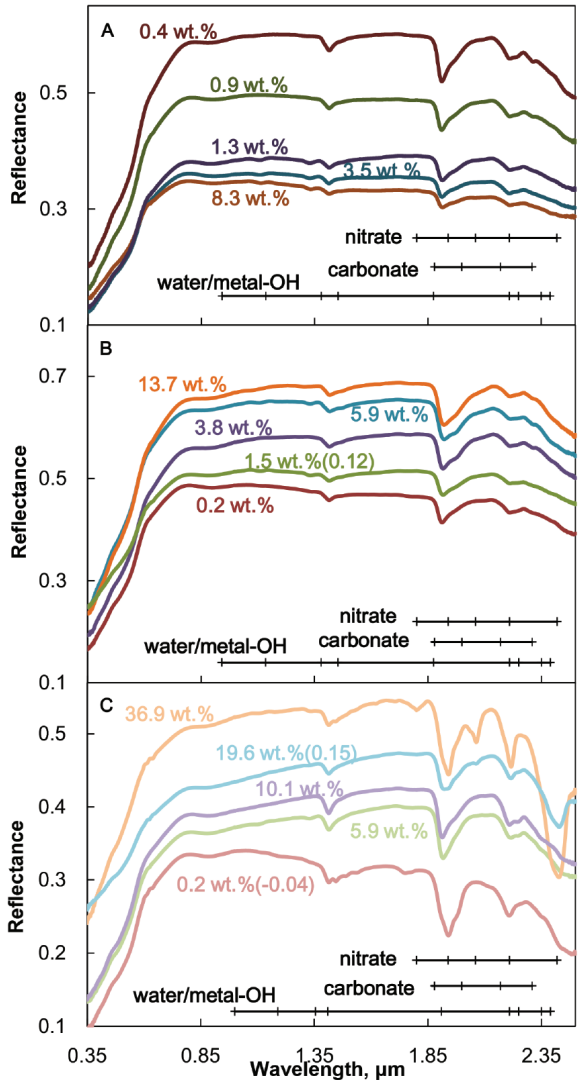

Figure 4. Representative laboratory reflectance spectra of regolith samples from the LT (**a**), ST (**b**), and CCP (**c**) profiles. The positions of absorption features of nitrate, carbonate, and water/metal-OH as shown in Table 2 are indicated by bars in the bottom of the charts. The numbers in weight percent delineate the nitrate contents in the regolith samples. The spectra are arranged according to nitrate contents with some spectra offset by a factor (positive: additive, negative: minus) listed in the parentheses in the chart.

contents and the 2.42 μm absorption band depths. The resulted correlation equation shown in Figure 5f should be applicable to quantify the nitrate contents based on the spectral properties of 2.42 μm band. There is also a significant positive correlation between the chloride contents and 2.42 μm band depths in the CCP profile ($p < 0.05$, Table 3), likely due to the significant correlation between chloride and nitrate contents (Pearson correlation coefficient: 0.85, $p < 0.001$) because of their similar solubilities that lead to similar transport activities and fate in the profile. Instead, no significant positive correlation was found between sulfate contents and the 2.42 μm absorption band depths in any of the three profiles (Table 3). Also, there is a significant negative correlation or no correlation between chloride/nitrate/sulfate contents and the band depths of the 1.81, 1.94, or 2.21 μm absorption features in the three profiles (Table 3), suggesting that other components rather than chloride/nitrate/sulfate mainly account for these features in these Atacama samples.

Therefore, the five nitrate absorption features in the VNIR region can provide general perspectives into the presence or absence of nitrate, and the appearance of 1.81 and 2.06 μm features and the absorption trough around 2.42 μm are typically indicative of large abundances of nitrate. The 2.42 μm can further be used to quantify nitrate contents in samples, especially when nitrate contents are >10 wt%.

Field-based spectral characterization of the Atacama nitrate mine regions

The field spectra have significant atmospheric absorptions around 1.4 and 1.9 μm compared to the laboratory spectra but are consistent with laboratory spectra with most nitrate absorption features prominent (except the 1.81 μm feature mostly disturbed by atmospheric absorptions) (Fig. 6). The similarity of Baquedano pit 1 to the LT and ST sites in nitrate contents is evident by their similar spectra with sporadic 1.94 μm absorptions, insignificant 2.06 μm shoulders, identifiable 2.21 μm absorptions and subtle inflections around 2.42 μm (Figs. 4a, 4b, 6a, and 6c). In contrast, for some samples from the Baquedano, Sierra Gorda, and Tama mine sites, there are clearly defined absorption features at 1.94, 2.06, and 2.21 μm, distinct inflections (even troughs) at ~2.42 μm, and sporadic absorptions around 1.81 μm in both the laboratory and field reflectance spectra, suggesting relatively high concentrations of nitrate at these three mine tailing sites (Figs. 6b and 6d–6h). In the Salar de Carmen, there are small but identifiable absorption bands around 1.94 and 2.21 μm, shoulders around 2.06 μm and inflections at ~2.42 μm in some of the field spectra, which together suggested an abundance of nitrate on the surface (Fig. 6i). This is consistent with past observations from Whitehead (1920) that proposed the natural efflorescence of sodium nitrate over a large area of the Salar de Carmen. Besides, in view of the yellowish color of the surface, significant absorptions in the ranges of 0.35–0.6 and 0.7–1.3 μm (centered at ~0.9 μm) are robust indications of iron (III). The 1.81 and 1.94 μm features in the spectra collected in the Salar de Grande are greatly influenced by atmospheric absorption and difficult to identify (Fig. 6j). The 2.06 μm features are almost absent, suggesting relatively low nitrate contents, in line with Stoertz and Ericksen (1974) that the Salar de Grande is dominated by halite minerals. Among these field spectra, one for the Tama mine has a complete set of five absorption features (Fig. 6f, black line), indicating the presence of the highest nitrate content. Considering the long wavelength side of the 2.42 μm absorption is subject to significant interferences of instrument noise, its absorption band depth was calculated to be the differences between the maximum and the minimum on the short wavelength side of the 2.42 μm continuum-removed absorption band (2.25–2.45 μm range). Based on the quantitative relationship demonstrated in Figure 5f, the largest 2.42 μm absorption band depth of 0.33 occurring at the Tama site corresponds to 35.7 wt% nitrate, which is consistent with the reported concentration range for the nitrate ores by Ericksen (1981); the samples from the Baquedano mine, Sierra Gorda mine, Tama mine, and the Salar de Carmen sites are mostly rich in nitrate with nitrate

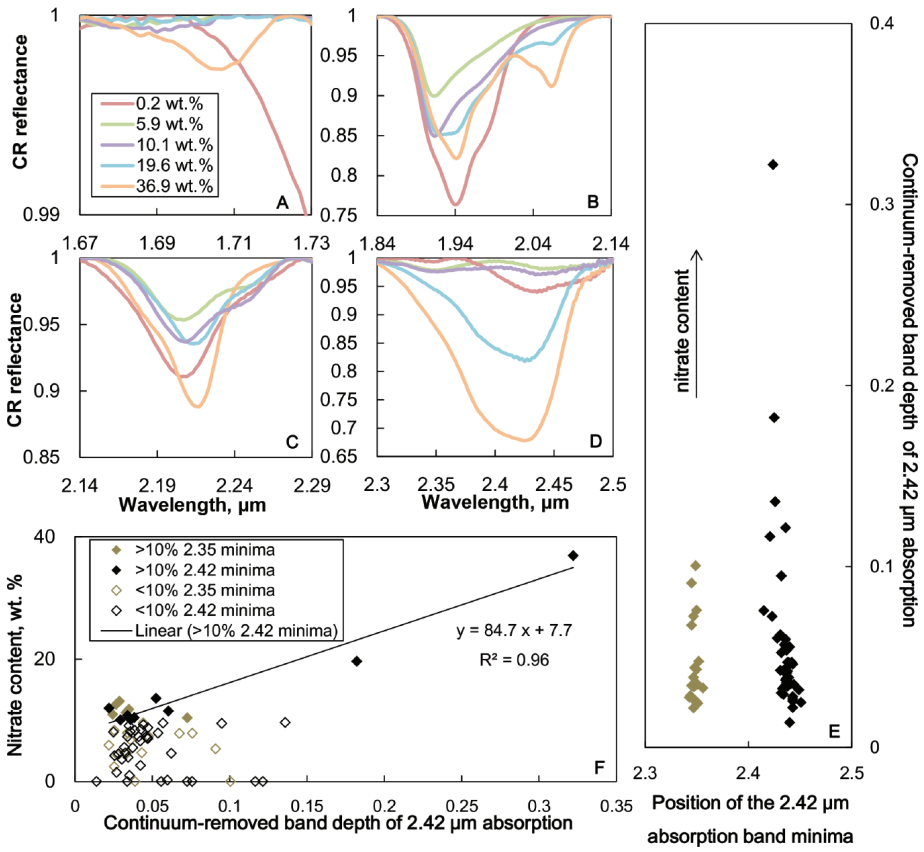

FIGURE 5. (**a**–**d**) Continuum-removed (CR) laboratory reflectance spectra of the selected CCP samples (the same as shown in Fig. 4c) in different spectral regions with isolated absorption features. (**e**) Points showing the exact wavelengths of the 2.42 µm absorption band minima, between 2.34 and 2.45 µm, vs. the band depth. (**f**) Continuum-removed band depths of 2.42 µm feature vs. nitrate contents in the CCP profile, with the solid line delineating the fitting line for the samples of nitrate contents >10 wt% and the band minima occurring at ~2.42 µm. The uncertainty in the position of the 2.42 µm absorption band minima is ≤10 nm.

contents generally >10 wt% (Fig. 7). In summary, this work suggests that in situ detection of nitrate is feasible using the field VNIR reflectance spectra by identifying some or all of the five nitrate absorption features, and the 2.42 µm absorption feature could even be used to determine the nitrate contents, showing great potential in implications into nitrate search and quantification on planetary surfaces via remote sensing techniques.

TABLE 3. Coefficients of Pearson correlation between anion contents and continuum-removed band depths of nitrate absorption features for the Atacama regolith samples

Contents	Continuum-removed band depths (µm)			
	1.81	1.94	2.21	2.42
		LT profile		
Chloride	–0.04	**–0.60[b]**	**–0.42[b]**	0.10
Nitrate	–0.03	**–0.52[b]**	**–0.40[b]**	0.20
Sulfate	0.03	–0.28	**–0.43[b]**	0.15
		ST profile		
Chloride	–0.18	–0.15	**–0.46[b]**	–0.09
Nitrate	–0.20	–0.16	**–0.43[b]**	–0.14
Sulfate	**–0.38[b]**	**–0.31[a]**	**–0.60[b]**	**–0.34[a]**
		CCP profile		
Chloride	**–0.32[b]**	**–0.33[b]**	–0.16	**0.30[a]**
Nitrate	**–0.28[a]**	**–0.27[a]**	–0.07	**0.53[b]**
Sulfate	0.23	0.09	–0.08	–0.12

Notes: The values in bold indicate the existence of significant correlations between absorption band depths and anion contents.
[a] Indicates the significant level <0.05, while [b] indicates the significant level <0.01.

IMPLICATIONS

The recent detection of nitrate, a biochemically accessible form of nitrogen, by the Mars Science Laboratory Curiosity rover adds to the evidence for the habitability of the ancient martian environment (Stern et al. 2015). Nitrate is naturally added to soils via atmospheric deposition or produced in situ via biological nitrification on Earth. Nitrification, the oxidation of ammonium via nitrifying bacteria, is generally considered to be the dominant mechanism of nitrate accumulation in most soils. Nevertheless, in hyper-arid regions such as the Atacama Desert, the Antarctic McMurdo Dry Valley and the Turpan-Hami basin, stable isotope technique proved that soil nitrate is predominantly from atmospheric deposition in that nitrification is minimized due to the lack of liquid water (Michalski et al. 2004; Qin et al. 2012; Wang et al. 2016). Though the martian nitrate discovered was also likely produced in the atmosphere rather than biology (Stern et al. 2015), the presence of nitrate suggests the potential evolution of the nitrogen cycle on the martian surface, which could instead provide fixed nitrogen essential for life. Therefore, the discovery of nitrate, together with the evidence of other life-related ingredients like liquid water (Ojha et al. 2015) and organic matter (Freissinet et al. 2015), suggests that Mars might have been more hospitable in the ancient past.

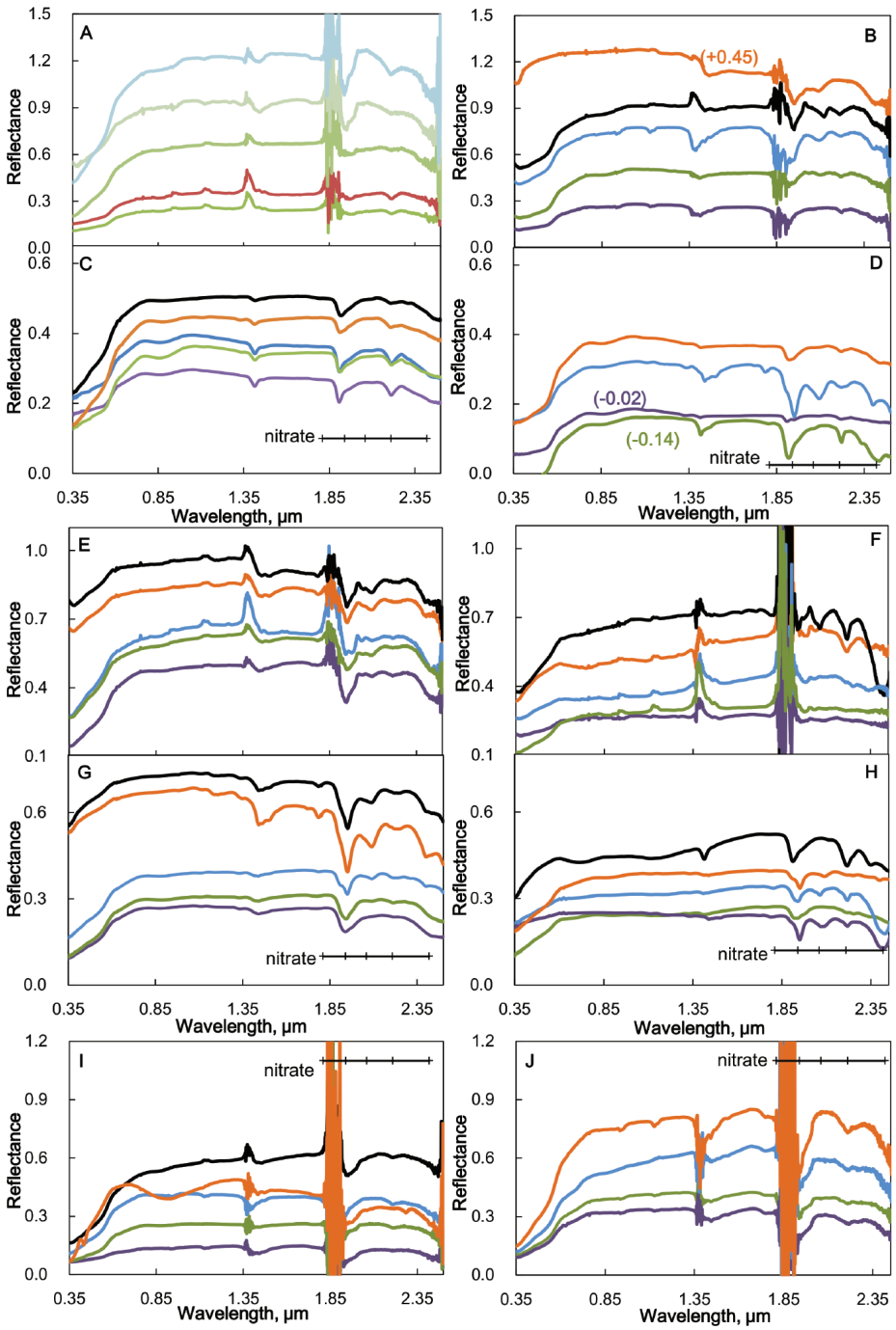

FIGURE 6. Representative reflectance spectra collected in the field: (**a**) Baquedano pit 1, (**b**) Baquedano mine, (**e**) Sierra Gorda mine, (**f**) Tama mine, (**i**) Salar de Carmen, (**j**) Salar de Grande. In the laboratory for returned samples: (**c**) Baquedano pit 1, (**d**) Baquedano mine, (**g**) Sierra Gorda mine, (**h**) Tama mine. The significant absorptions around 1.4 and 1.9 µm in the field spectra are caused by atmospheric water. The positions of nitrate absorptions are indicated by the bars in the charts. The spectra are arranged for clarity with some spectra offset by a factor (positive: additive; negative: minus) listed in the parentheses in the charts.

If any past martian environments were habitable, they probably existed billions of years ago, when atmospheric nitrogen (as N_2) was estimated to be 3–300 mbar, far higher than the present-day martian atmosphere of ~0.2 mbar (Mancinelli 1996). If there was abundant nitrogen, where has it gone? Conversion of N_2 into nitrate by fixation and its storage in the martian regolith is one possibility. Exploration of nitrate mineral distributions could determine which fixation process was most important, and identifying the coexisting mineral assemblages should improve our understanding of pedogenesis and atmospheric chemistry on Mars.

This study lays the groundwork for mapping nitrates on Mars, and will supplement existing spectral libraries and provide suitable criteria for identification of different nitrate minerals using hyperspectral sensors. Progress toward mapping astrobiologically

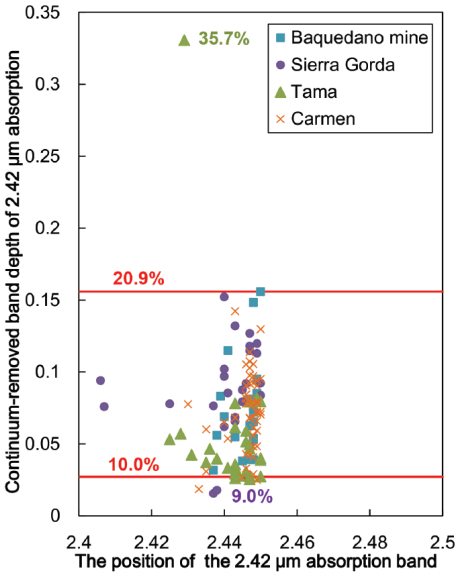

FIGURE 7. Points showing the exact wavelengths of the band minima vs. the continuum-removed band depths of the 2.42 µm absorption for the field spectra collected in the Atacama nitrate mine regions. The numbers in the chart delineate the nitrate contents corresponding to the absorption band depths of the red lines or points based on the quantitative relationship shown in Figure 5f. The uncertainty in the position of the 2.42 µm absorption band minima is ≤10 nm.

important nitrate via orbital spectroscopy will have important implications for surface processes, propose future martian missions where nitrate is a priority, and eventually help with the seeking for life on Mars. Considering nitrate and chloride salts have similar solubility and the common co-occurrence of nitrate and chloride minerals at Mars analog sites (Ericksen 1981; Qin et al. 2012), the nitrate search will first be advised to follow the chloride deposits on Mars. Future martian nitrate detection will be augmented by several upcoming landed spectrometers, i.e., MicrOMEGA (0.9–3.5 µm range, 20 nm resolution) (Leroi et al. 2009) and MA_MISS (0.8–2.8 µm range, 20 nm resolution) (Coradini et al. 2001), which will both be equipped with the ESA 2018 ExoMars rover, as well as the SuperCam (0.4–0.9 µm range, <1 nm resolution and 1.3–2.6 µm range, 0.02 µm resolution) that will fly on the 2020 Mars rover (Wiens et al. 2017), and their synergies with the complementary microscopy and chemical analysis techniques.

ACKNOWLEDGMENTS

The data collection was partially supported by the U.S. National Science Foundation Grant (EAR 0922114) to G.M., the Mineralogical Society of America Graduate Student Research Grant to F.W., and several fellowships from Purdue University to F.W. (Purdue Climate Change Research Center fellowship, Purdue Research Foundation research assistantship and Purdue Bilsland Dissertation fellowship). The data analysis and paper writing were mainly conducted at Peking University Shenzhen Graduate School supported by the postdoctoral funding from Peking University Shenzhen Graduate School. We thank Raul Ochoa for his assistance in the lab and field. We are also grateful to Keith Putirka (editor), Javier Cuadros (associate editor), and two reviewers for valuable suggestions that helped greatly improve this paper.

REFERENCES CITED

Banin, A., Han, F.X., Kan, I., and Cicelsky, A. (1997) Acidic volatiles and the Mars soil. Journal of Geophysical Research-Planets, 102, 13,341–13,356.

Bao, H.M., and Gu, B.H. (2004) Natural perchlorate has a unique oxygen isotope signature. Environmental Science and Technology, 38, 5073–5077.

Bao, H., Jenkins, K.A., Khachaturyan, M., and Dıáz, G.C. (2004) Different sulfate sources and their post-depositional migration in Atacama soils. Earth and Planetary Science Letters, 224, 577–587.

Boonmung, S., and Riley, M.R. (2003) Quantitative analysis of added ammonium and nitrate in silica sand and soil using diffuse reflectance infrared spectroscopy. Spectroscopy Letters, 36, 251–274.

Clark, R.N., King, T.V.V., Klejwa, M., Swayze, G.A., and Vergo, N. (1990) High spectral resolution reflectance spectroscopy of minerals. Journal of Geophysical Research: Solid Earth, 95(B8), 12653–12680.

Clark, R.N., Swayze, G.A., Wise, R., Livo, E., Hoefen, T., Kokaly, R., and Sutley, S.J. (2007) USGS digital spectral library splib06a: U.S. Geological Survey, Digital Data Series 231. U.S. Geological Survey, Denver, Colorado, http://speclab.cr.usgs.gov/spectral.lib06 (accessed October 15, 2016).

Cloutis, E.A., Hawthorne, F.C., Mertzman, S.A., Krenn, K., Craig, M.A., Marcino, D., Methot, M., Strong, J., Mustard, J.F., Blaney, D.L., Bell, J.F., and Vilas, F. (2006) Detection and discrimination of sulfate minerals using reflectance spectroscopy. Icarus, 184, 121–157.

Cloutis, E., Berg, B., Mann, P., and Applin, D. (2016) Reflectance spectroscopy of low atomic weight and Na-rich minerals: borates, hydroxides, nitrates, nitrites, and peroxides. Icarus, 264, 20–36.

Coradini, A., Piccinoni, G., Amici, S., Bianchi, R., Capaccioni, F., Capria, M.T., De Sanctis, M.C., Di Lellis, A.M., Espinasse, S., Federico, C., and others. (2001) MA_MISS: Mars multispectral imager for subsurface studies. Advances in Space Research, 28, 1203–1208.

Crowley, J.K. (1991) Visible and near-infrared (0.4-2.5 µm) reflectance spectra of playa evaporite minerals. Journal of Geophysical Research: Solid Earth, 96, 16231–16240.

Ehsani, M.R., Upadhyaya, S.K., Fawcett, W.R., Protsailo, L.V., and Slaughter, D. (2001) Feasibility of detecting soil nitrate content using a mid-infrared technique. Transactions of the Asae, 44, 1931–1940.

Ericksen, G.E. (1981) Geology and origin of the Chilean nitrate deposits. U.S. Geological Survey Professional Paper 1188, 37 p.

Ericksen, G.E., and Mrose, M.E. (1970) Mineralogical studies of the nitrate deposits of Chile. II. Darapskite, $Na_3(NO_3)(SO_4)\cdot H_2O$. American Mineralogist, 55, 1500–1517.

Ewing, S., Sutter, B., Owen, J., Nishiizumi, K., Sharp, W., Cliff, S., Perry, K., Dietrich, W., McKay, C., and Amundson, R. (2006) A threshold in soil formation at Earth's arid-hyperarid transition. Geochimica et Cosmochimica Acta, 70, 5293–5322.

Freissinet, C., Glavin, D.P., Mahaffy, P.R., Miller, K.E., Eigenbrode, J.L., Summons, R.E., Brunner, A.E., Buch, A., Szopa, C., Archer Jr., P.D., and others and the MSL Science Team (2015), Organic molecules in the Sheepbed Mudstone, Gale Crater, Mars. Journal of Geophysical Research-Planets, 120, 495–514.

Gendrin, A., Mangold, N., Bibring, J.P., Langevin, Y., Gondet, B., Poulet, F., Bonello, G., Quantin, C., Mustard, J., Arvidson, R., and LeMouélic, S. (2005) Sulfates in Martian layered terrains: the OMEGA/Mars Express view. Science, 307, 1587–1591.

Hanley, J., Dalton, J.B., Chevrier, V.F., Jamieson, C.S., and Barrows, R.S. (2015) Reflectance spectra of hydrated chlorine salts: the effect of temperature with implications for Europa. Journal of Geophysical Research Planets, 119, 2370–2377.

Harris, M.J., Salje, E.K.H., and Güttler, B.K. (1990) An infrared spectroscopic study of the internal modes of sodium nitrate: implications for the structural phase transition. Journal of Physics: Condensed Matter, 2, 5517–5527.

Hathaway, B.J., Holah, D.G., and Hudson, M. (1963) The infrared and reflectance spectra of some transition-metal nitrate and perchlorate dihydrates. Journal of the Chemical Society, 4586–4589.

Hecht, M.H., Kounaves, S.P., Quinn, R.C., West, S.J., Young, S.M.M., Ming, D.W., Catling, D.C., Clark, B.C., Boynton, W.V., Hoffman, J.L., and others. (2009) Detection of perchlorate and the soluble chemistry of Martian soil at the Phoenix lander site. Science, 325, 64–67.

Houston, J. (2006) Variability of precipitation in the Atacama Desert: Its causes and hydrological impact. International Journal of Climatology, 26, 2181–2198.

Houston, J., and Hartley, A.J. (2003) The central Andean west slope rainshadow and its potential contribution to the origin of hyper-aridity in the Atacama Desert. International Journal of Climatology, 23, 1453–1464.

Hovis, W.A. (1966) Infrared spectral reflectance of some common minerals. Applied Optics, 5, 245–248.

Hunt, G.R. (1977) Spectral signatures of particulate minerals in the visible and near infrared. Geophysics, 42, 501–513.

Jahn, B.R., Linker, R., Upadhyaya, S.K., Shaviv, A., Slaughter, D.C., and Shmulevich, I. (2006) Mid-infrared spectroscopic determination of soil nitrate content. Biosystems Engineering, 94, 505–515.

Kokaly, R.F., and Clark, R.N. (1999) Spectroscopic determination of leaf biochemistry using band-depth analysis of absorption features and stepwise multiple linear regression. Remote Sensing of Environment, 67, 267–287.

Leroi, V., Bibring, J.P., and Berthe, M. (2009) Micromega/IR: Design and status of a near-infrared spectral microscope for in situ analysis of Mars samples. Planetary and Space Science, 57, 1068–1075.

Mancinelli, R.L. (1996) The search for nitrogen compounds on the surface of Mars. Pergamon Press Ltd, Oxford.
Michalski, G., Böhlke, J.K., and Thiemens, M. (2004) Long term atmospheric deposition as the source of nitrate and other salts in the Atacama Desert, Chile: New evidence from mass-independent oxygen isotopic compositions. Geochimica et Cosmochimica Acta, 68, 4023–4038.
Moorcroft, M.J., Davis, J., and Compton, R.G. (2001) Detection and determination of nitrate and nitrite: a review. Talanta, 54, 785–803.
Nair, H., Allen, M., Anbar, A.D., Yung, Y.L., and Clancy, R.T. (1994) A photochemical model of the Martian atmosphere. Icarus, 111, 124–150.
Navarro-González, R., Rainey, F., Molina, P., Bagaley, D., Hollen, B., de la Rosa, J., Small, A., Quinn, R., Grunthaner, F., and Caceres, L. (2003) Mars-like soils in the Atacama Desert, Chile, and the dry limit of microbial life. Science, 302, 1018–1021.
Ojha, L., Wilhelm, M.B., Murchie, S.L., McEwen, A.S., Wray, J.J., Hanley, J., Massé, M. and Chojnacki, M. (2015) Spectral evidence for hydrated salts in recurring slope lineae on Mars. Nature Geoscience, 8, 829–832.
Osterloo, M.M., Hamilton, V.E., Bandfield, J.L., Glotch, T.D., Baldridge, A.M., Christensen, P.R., Tornabene, L.L., and Anderson, F.S. (2008) Chloride-bearing materials in the southern highlands of Mars. Science, 319, 1651–1654.
Qin, Y., Li, Y., Bao, H., Liu, F., Hou, K., Wan, D., and Zhang, C. (2012) Massive atmospheric nitrate accumulation in a continental interior desert, northwestern China. Geology, 40, 623–626.
Seinfeld, J.H., and Pandis, S.N. (2006) Atmospheric Chemistry and Physics: From air Pollution to Climate Change. Wiley.
Sinfield, J.V., Fagerman, D., and Colic, O. (2010) Evaluation of sensing technologies for on-the-go detection of macro-nutrients in cultivated soils. Computers and Electronics in Agriculture, 70, 1–18.
Squyres, S.W., Grotzinger, J.P., Arvidson, R.E., Bell, J.F., Calvin, W., Christensen, P.R., Clark, B.C., Crisp, J.A., Farrand, W.H., Herkenhoff, K.E., and others. (2004) In situ evidence for an ancient aqueous environment at Meridiani Planum, Mars. Science, 306, 1709–1714.
Stern, J.C., Sutter, B., Freissinet, C., Navarro-González, R., McKay, C.P., Douglas, P.A., Buch, A., Brunner, A.E., Coll, P., Eigenbrode J.L., and others. (2015) Evidence for indigenous nitrogen in sedimentary and aeolian deposits from the Curiosity rover investigations at Gale crater, Mars. Proceedings of the National Academy of Sciences, 112, 4245–4250.
Stern, J.C., Sutter, B., Jackson, W.A., Navarro-González, R., Mckay, C.P., Ming, D.W., Archer, P.D., and Mahaffy, P.R. (2017) The nitrate/(per)chlorate relationship on Mars. Geophysical Research Letters, 44, 2643–2651.
Stoertz, G.E., and Ericksen, G.E. (1974) Geology of salars in northern Chile. U.S. Geological Survey Professional Paper, 811, 65 p.
Sutter, B., Dalton, J., Ewing, S.A., Amundson, R., and McKay, C.P. (2007) Terrestrial analogs for interpretation of infrared spectra from the Martian surface and subsurface: sulfate, nitrate, carbonate, and phyllosilicate-bearing Atacama Desert soils. Journal of Geophysical Research, 112, G04S10.
Wang, F., Michalski, G., Seo, J.H., Granger, D.E., Lifton, N., and Caffee, M. (2015) Beryllium-10 concentrations in the hyper-arid soils in the Atacama Desert, Chile: Implications for arid soil formation rates and El Niño driven changes in Pliocene precipitation. Geochimica et Cosmochimica Acta, 160, 227–242.
Wang, F., Ge, W.S., Luo, H., Seo, J.H., and Michalski, G. (2016) Oxygen-17 anomaly in soil nitrate: A new precipitation proxy for desert landscapes. Earth and Planetary Science Letters, 438, 103–111.
Watters, W.A., Grotzinger, J.P., Bell, J., Grant, J., Hayes, A.G., Li, R.X., Squyres, S.W., and Zuber, M.T. (2011) Origin of the structure and planform of small impact craters in fractured targets: Endurance Crater at Meridiani Planum, Mars. Icarus, 211, 472–497.
Whitehead, W.L. (1920) The Chilean nitrate deposits. Economic Geology, 15, 187–224.
Wiens, R.C., Maurice, S., and Perez, F.R. (2017) The SuperCam remote sensing instrument suite for the mars 2020 rover: A preview. Spectroscopy (Santa Monica), 32, 50–55.
Xu, M., Larentzos, J.P., Roshdy, M., Criscenti, L.J., and Allen, H.C. (2008) Aqueous divalent metal-nitrate interactions: hydration versus ion pairing. Physical Chemistry Chemical Physics, 10, 4793–4801.
Yung, Y.L., Strobel, D.F., Kong, T.Y., and McElroy, M.B. (1977) Photochemistry of nitrogen in martian atmosphere. Icarus, 30, 26–41.

Manuscript received March 17, 2017
Manuscript accepted October 3, 2017
Manuscript handled by Javier Cuadros

Endnote:

[1]Deposit item AM-18-26141, Supplemental Material. Deposit items are free to all readers and found on the MSA web site, via the specific issue's Table of Contents (go to http://www.minsocam.org/MSA/AmMin/TOC/2018/Feb2018_data/Feb2018_data.html).